


Generating Controllable Laguerre-Gaussian Laser Modes Through Intracavity Spin-Orbital Angular Momentum Conversion of Light

Dunzhao Wei,¹ Yue Cheng,¹ Rui Ni,¹ Yong Zhang,^{1,*} Xiaopeng Hu,^{1,†} Shining Zhu,¹ and Min Xiao^{1,2,‡}

¹*National Laboratory of Solid State Microstructures, College of Engineering and Applied Sciences, and School of Physics, Nanjing University, Nanjing 210093, China*

²*Department of Physics, University of Arkansas, Fayetteville, Arkansas 72701, USA*

 (Received 11 September 2018; revised manuscript received 25 December 2018; published 18 January 2019)

The rapid developments in orbital-angular-momentum-carrying Laguerre-Gaussian (LG_l^0) modes in recent years have facilitated progress in optical communication, micromanipulation, and quantum information. However, it is still challenging to efficiently generate bright, pure, and selectable LG_l^0 laser modes in compact devices. We demonstrate a low-threshold solid-state laser that can directly output selected high-purity LG_l^0 modes with high efficiency and controllability. Spin-orbital angular momentum conversion of light is used to reversibly convert the transverse modes inside a cavity and determine the output mode index. The generated LG_1^0 and LG_2^0 laser modes have purities of approximately 97% and approximately 93% and slope efficiencies of approximately 11% and approximately 5.1%, respectively. Our cavity design can also be easily extended to produce higher-order Laguerre-Gaussian modes and cylindrical vector beams. Such a compact laser configuration features flexible control, low threshold, and robustness, making it a practical tool for applications in superresolution imaging, high-precision interferometers, and quantum correlations.

DOI: [10.1103/PhysRevApplied.11.014038](https://doi.org/10.1103/PhysRevApplied.11.014038)

I. INTRODUCTION

Laguerre-Gaussian (LG_l^p) modes, characterized by the azimuthal index l (any integers) and the radial index p (zero or positive integers), are the eigen solutions of the paraxial wave equation in cylindrical coordinates [1]. These LG_l^p modes form a complete and orthonormal set, so that an arbitrary spatial light field can be expressed as the superposition of LG_l^p modes [2]. The LG_l^p modes with $p=0$, as special optical vortices, have been a hot research topic since the orbital angular momentum (OAM) properties of light beams were identified in the azimuthal phase term $e^{il\varphi}$ of the LG_l^0 modes [3]. The LG_l^0 mode carries an OAM of $l\hbar$ per photon, where \hbar is the reduced Planck constant and l is also called a topological charge (TC). Featuring donut-shaped intensity distributions and carrying OAM, the LG_l^0 modes have been widely applied in optical tweezers, nonlinear and quantum optics, optical communication, superresolution imaging, material processing, rotation Doppler effect, and so on [4–15]. The evolving practical applications inevitably require high-quality LG_l^p laser modes. For example, a pure LG_l^0 mode has a more uniform donut-intensity distribution along

the propagation direction, which can increase the depth resolution in superresolution imaging [16]. In the field of precision measurement, it has been shown that higher-order LG_l^p modes can reduce thermal noise in the LIGO system for gravitational-wave detection because of their more homogeneous power distributions [17,18]. The high-precision optical interferometry in the laser interferometer gravitational-wave observatory (LIGO) system requires a high-purity LG_l^p mode. In quantum information science, high-purity LG_l^p modes could increase hybrid azimuthal-radial quantum correlations [19–21]. However, it is still a challenge to efficiently generate high-purity LG_l^p modes in a simple optical setting. We experimentally demonstrate an intracavity spin-orbital angular-momentum conversion method to produce selected high-purity LG_l^0 laser modes, which can be feasibly extended to generate other LG_l^p laser modes.

The common way to generate a LG_l^0 beam is to add the azimuthal phase term of $e^{il\varphi}$ to a Gaussian mode using a fork-grating, a q plate, a spiral phase plate, and so on [22]. However, directly adding a spiral phase to the Gaussian mode will generate a hypergeometric-Gaussian (HyGG) mode with a definite l index, but with an expansion of the p index [23,24]. The multiple p components decrease the mode purity and conversion efficiency of the desired LG_l^0 beam. Furthermore, the power weightings of these undesired LG_l^p (with $p > 0$) modes have positive

*zhangyong@nju.edu.cn

†xphu@nju.edu.cn

‡mxiao@uark.edu

correlations to the modulus of the l index. These undesired radial modes hidden in the LG_l^0 beam will decrease the imaging resolution in a superresolution microscope, reduce the accuracy of a high-precision interferometer [25], contaminate quantum information processing [19,20], and induce uncertainties in nonlinear interactions [26].

Researchers have turned to intracavity modulation for generating high-purity LG_l^0 modes, since an optical cavity can perform mode selection and directly output laser modes [27,28]. Unfortunately, because LG_l^0 modes with opposite handedness (for example, $l=1$ and $l=-1$ modes) have the same loss and are degenerate in an active optical cavity, their coherent superpositions usually form petal-intensity patterns [29,30]. The superposition of two petal-intensity patterns may form a donut-intensity profile, but not a pure LG_l^0 mode [31]. Special components, such as nanoscale stripes and oblique etalons, are proposed to discriminate the degenerate LG_l^0 modes inside active cavities. However, the additional components with circular asymmetries spoil the mode purities of the generated LG_l^0 modes, which has impeded their further development [32,33]. Recently, q plates, a kind of planar phase-modulation device, are utilized inside the laser cavity for generating high-purity LG_l^0 modes [34]. However, the impractical laser parameters, such as the extremely high pump power needed for operation, severely limits its further applications [34]. To generate useful LG_l^0 laser modes with high mode purities, low lasing thresholds, and controllable mode indices, the laser cavity needs to be carefully designed with proper control and selection of intracavity components.

In our experiment, we put a vortex half-wave plate (VWP, Thorlabs, Inc.), a Faraday rotator (FR), and a quarter-wave plate (QWP) inside a Nd:YVO₄ laser cavity, which can achieve cavity mode reversibility through intracavity spin-orbital angular-momentum conversion. The process is self-producing after each round trip. The QWP generates a circularly polarized state carrying a spin angular momentum (SAM) of $\pm\hbar$ per photon depending on its handedness [35]. The interaction between a photon and an optically anisotropic medium will change the value of the photon's SAM and induce a geometric phase shift [36]. The VWP, featuring the artificial helical anisotropic parameter space, can add a spiral geometric phase to an incident mode by flipping the handedness of its circular polarization, i.e., spin-orbital angular-momentum conversion. Therefore, the VWP converts the SAM or polarization of the intracavity field into the OAM, and flexibly controls the TC [37]. The modulus and sign of the TC can be changed by using different VWPs and rotating the QWP, respectively. Since the intracavity spin-orbital angular-momentum conversion requires the cavity mode to evolve from a Gaussian shape at the front mirror to a desired LG mode at the output mirror, it is essential to guarantee the effective mode conversion in cavity design.

By carefully optimizing the cavity mode to match the unique requirements of each intracavity component, the laser outputs a selected high-purity LG_l^0 laser mode, for example, a LG_1^0 (LG_2^0) mode with a mode purity of approximately 97% (approximately 93%), at a wavelength of 1064 nm in our experiment. The specially designed compact cavity requires only a few intracavity components, which benefits the system stability, loss control, and practical operation. The lasing thresholds for lower-order LG_l^0 modes are comparable to that of the Gaussian mode and the slope efficiencies of the LG_1^0 and LG_2^0 lasing modes are approximately 11% and approximately 5.1%, respectively. The beam quality factor and mode stability at high pump power also show the excellent laser performance. The flexibility of the cavity design is also reflected in its ability to generate laser outputs of vector beams with cylindrical symmetry in polarization by slightly modifying the intracavity elements [38].

II. MATERIALS AND METHODS

A. Working principle of the VWP

The VWP can be seen as a spatially variant half-wave plate, whose fast axis rotates continuously over the area of the optic around a singularity point. Its transmission efficiency is up to 96%. The orientation of its fast axis can be expressed as

$$\theta(\varphi) = \frac{m}{2}\varphi + \varphi_0, \quad (1)$$

where φ is the azimuthal angle, φ_0 is the orientation of the fast axis at $\varphi = 0$, and m is a positive integer determined by the VWP. Its Jones matrix can be written as [37]

$$M(\theta) = \begin{bmatrix} \cos 2\theta & \sin 2\theta \\ \sin 2\theta & -\cos 2\theta \end{bmatrix}. \quad (2)$$

If we apply it to a horizontally polarized light beam, the output result can be expressed as

$$E_V = M(\theta) \begin{pmatrix} 1 \\ 0 \end{pmatrix} = \begin{bmatrix} \cos(m\varphi + 2\varphi_0) \\ \sin(m\varphi + 2\varphi_0) \end{bmatrix}. \quad (3)$$

Equation (3) shows that each point on the transverse plane of the output beam is linearly polarized, but the polarization direction depends on the azimuthal angle φ . Therefore, an input linearly polarized Gaussian mode will generate a cylindrical vector beam [38]. If we apply it to a left-circularly-polarized (LCP) or right-circularly-polarized (RCP) OAM mode with TC of l_0 :

$$\begin{cases} M(\theta) \times |l_0, L\rangle = |l_0 + m, R\rangle, \\ M(\theta) \times |l_0, R\rangle = |l_0 - m, L\rangle, \end{cases} \quad (4)$$

where L and R refer to the LCP and RCP states and both the SAM and OAM change during the process of the spin-orbital conversion. A LCP (or RCP) OAM mode with TC of l_0 passing through the VWP will become a RCP (or LCP) OAM mode with TC of $l_0 + m$ (or $l_0 - m$). When l_0 equals zero (e.g., the Gaussian mode), the TC will be controlled only by the m value of the VWP and the handedness of the incident circularly polarized beam.

B. Principle of intracavity spin-orbital angular-momentum conversion

In a stable laser cavity, a light beam should reproduce itself after each round trip when the cavity resonates. Since each point on the VWP is a half-wave retarder, a linearly polarized light beam, propagating forward and then reflecting backward through the same VWP, is equivalent to passing through a full-wave plate in which the initial polarization and wavefront are recovered [Fig. 1(a)]. To convert the spin and orbital angular momenta, a QWP is needed to turn the linearly polarized state to the circularly polarized state. The combination of the FR and QWP makes the light beam reversible when its initial polarization direction is parallel to the optical axis of the QWP [Fig. 1(b)]. Therefore, by combining the FR, QWP, and VWP, we achieve a complete reversible cycle inside a laser cavity for the output of a selected OAM-carrying

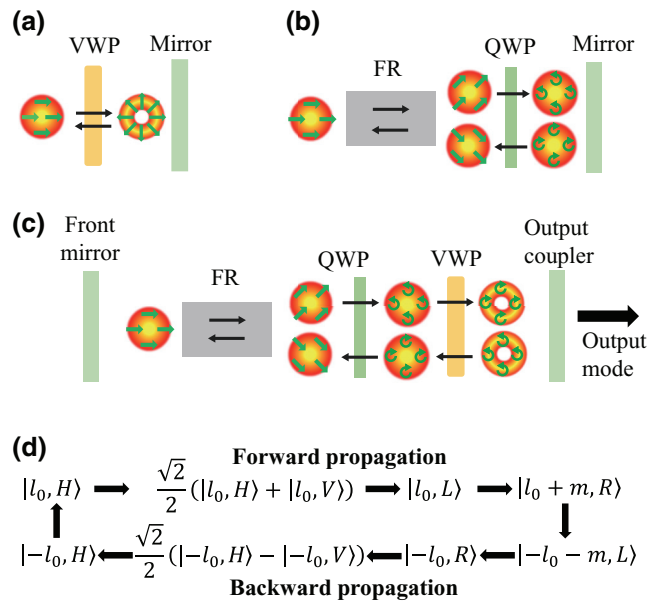


FIG. 1. Reversible light transmission in a laser cavity. (a) A reversible optical setup including a VWP and a mirror. (b) A reversible optical setup including a FR, a QWP, and a mirror. (c) A reversible optical cavity combining the FR, QWP, and VWP for OAM mode generation. (d) The complete reversible cycle of mode transformation in (c). Black arrows represent the propagation directions of light. Green arrows correspond to the polarization of light.

mode [Fig. 1(c)]. Here, the FR enables mode-reversible propagation. The system is greatly simplified in comparison to the previous intracavity geometric-phase-control configuration [34]. Figure 1(d) shows a one-round-trip mode transformation for the laser output of a $|l_0 + m, R\rangle$ mode in the configuration shown in Fig. 1(c). The configuration performs the transformation $|l_0, H\rangle \rightarrow |l_0 + m, R\rangle$ in the forward propagation and $|-l_0 - m, L\rangle \rightarrow |-l_0, H\rangle$ in the backward propagation, where H refers to the horizontally polarized state. The intracavity spin-orbital angular-momentum conversion happens when light passes through the VWP, i.e., $|l_0, L\rangle \rightarrow |l_0 + m, R\rangle$ for forward conversion and $|-l_0 - m, L\rangle \rightarrow |-l_0, R\rangle$ for backward conversion, considering that the reflection at the output coupler induces the inversions of handedness for both SAM and OAM. The additional TC of m is cancelled in a round trip to satisfy the reversible transformation in the cavity. In addition, orienting the fast axis of the QWP vertically, the forward conversion becomes $|l_0, H\rangle \rightarrow |l_0 - m, L\rangle$, which will output the $|l_0 - m, L\rangle$ mode. In our experiment, the cavity mode between the front mirror and the VWP carries a TC of $l_0 = 0$, so the TC of an output mode is directly

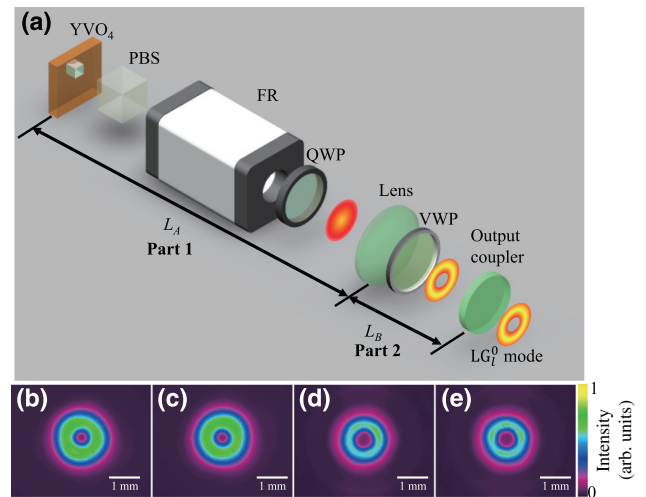


FIG. 2. Experimental setup and the output intensity patterns. (a) The experimental setup for generating LG_l^0 laser modes. An end-pumped solid-state laser comprised of a Nd:YVO₄ crystal, a lens, and an output coupler working at a wavelength of 1064 nm. The crystal is pumped by an 808-nm-wavelength fiber-coupled diode laser. Following the crystal, a PBS, a FR, a QWP, and a VWP are placed in the cavity successively for polarization state control and spin-orbital angular-momentum conversion. All of them have antireflection coatings and are oriented precisely so that the whole cavity satisfies the reversible propagation condition. (b),(c) are the output LG_1^0 and LG_{-1}^0 modes using a VWP of $m = 1$, respectively. (d),(e) are the output LG_2^0 and LG_{-2}^0 modes using a VWP of $m = 2$, respectively. These images are captured 50 cm away from the output coupler. From (b),(d), the measured diameters of the output LG_1^0 and LG_2^0 modes are 2 and 2.4 mm, respectively.

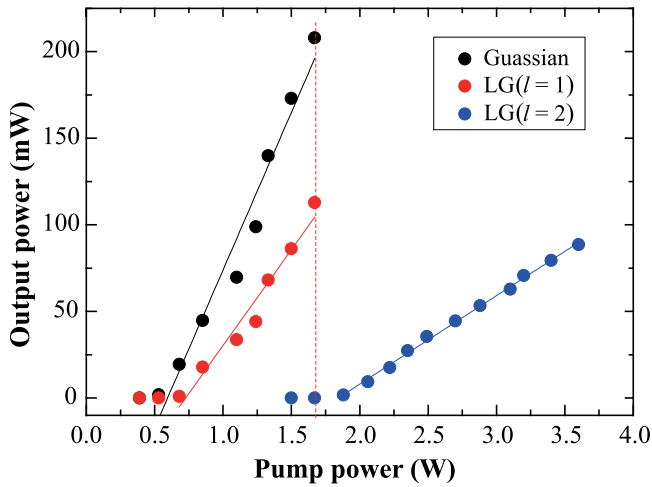


FIG. 3. Output powers vs the pump power. The experimentally measured output powers of the LG_0^0 , LG_1^0 , and LG_2^0 laser modes are shown by black, red, and blue dots, respectively. The corresponding fitting results are shown in colored lines.

controlled by the QWP and the VWP (see Appendix A for the self-reproducing process).

C. Laser cavity design

Figure 2(a) shows the experimental setup. An end-pumped solid-state laser, working in continuous-wave mode at a 1064-nm wavelength, is comprised of a Nd:YVO₄ crystal as the gain medium, a film coated on the front face of the crystal as a front mirror, a lens with a focal length f , and a partially transmitted plane mirror as an output coupler. The FR, QWP, and VWP are inserted into this laser cavity to achieve reversible mode conversion during spin-orbital conversion. The lens divides the

cavity into two parts [Part 1 and Part 2 in Fig. 2(a)] with lengths labelled as L_A and L_B , satisfying the cavity stability condition [39]

$$0 \leq \left(1 - \frac{L_A}{f}\right) \left(1 - \frac{L_B}{f}\right) \leq 1. \quad (5)$$

We choose to work under the conditions of $L_A < f$ and $L_B < f$. Considering the refractive indices of the gain medium, FR and QWP in the first part of the cavity, the actual L_A can be a bit larger than f without breaking the cavity stability condition. To optimize mode matching, L_A is set to approach f so that the cavity mode has a diameter large enough at the position of the lens and a diameter comparable to that of the pump beam at the position of the gain medium. In the cavity design, a Gaussian mode presents at the gain medium to match the pump laser mode. The pump beam is focused on the crystal with a 200- μm -diameter Gaussian spot. The VWP is placed in Part 2 of the cavity adjacent to the lens to take advantage of the large mode size. A polarization beam splitter (PBS) is inserted between the gain medium and the FR to eliminate the unwanted vertically polarized light caused by the imperfect polarization modulation from the FR, QWP, and VWP. A 1-mm-diameter pinhole is placed at the front of the output coupler to filter out the higher-order transverse modes so that the cavity can output the desired LG_l^0 beam. Therefore, in an ideal case with a highly efficient intracavity mode conversion, a LG_0^0 mode (i.e., Gaussian mode) is expected to oscillate in Part 1 of the cavity, while a LG_l^0 mode oscillates in the regime of Part 2. It should be noted that the actual cavity mode in Part 1 is not perfectly Gaussian because the VWP can only introduce a helical phase [23]. Under such an experimental configuration, higher- p -order LG modes are greatly suppressed and

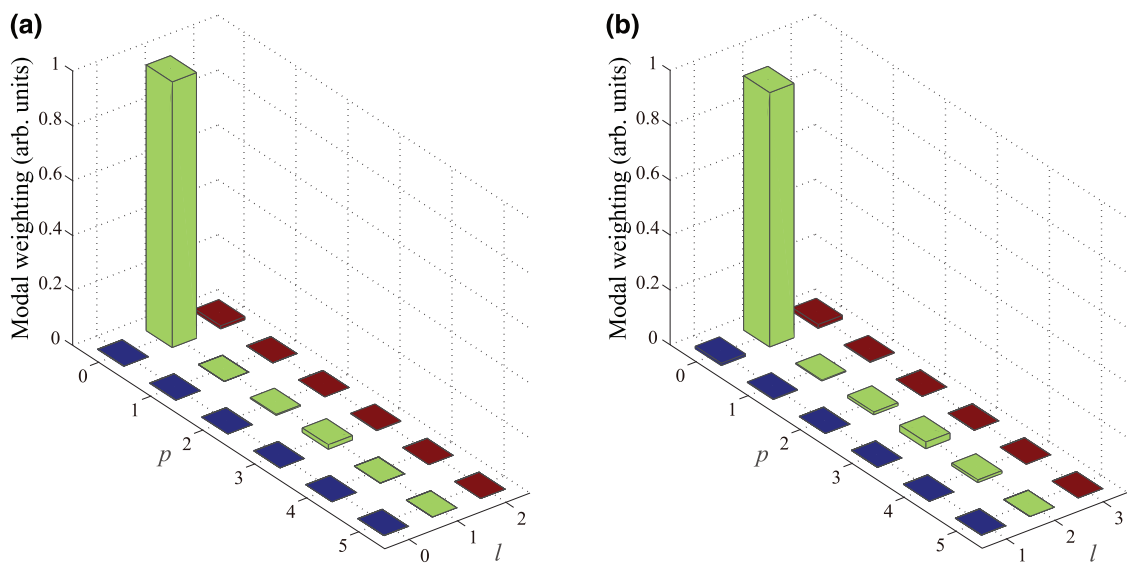


FIG. 4. Modal decomposition results. The modal decomposition results of the output LG_1^0 mode (a) and LG_2^0 mode (b), respectively.

the laser will output a selected high-purity circularly polarized LG_l^0 mode (see Appendix B for detailed information of the experimental setup). Figure 2(b) shows an output LG_1^0 laser mode generated by the VWP of $m = 1$. The LG_{-1}^0 mode can be generated [Fig. 2(c)] by rotating the QWP with an angle of 90° . Replacing the VWP with $m = 2$, we have generated the LG_2^0 (or LG_{-2}^0) mode by orienting the fast axis of the QWP horizontally (or vertically) as shown in Fig. 2(d) [or Fig. 2(e)]. All the intensity profiles present a high-quality donut shape. Since the experimental setup is similar for generating RCP $LG_{|l|}^0$ and LCP $LG_{-|l|}^0$ modes, we will only present the laser properties of RCP LG_1^0 and LG_2^0 laser modes in the following.

III. RESULTS AND DISCUSSION

A. Lasing threshold and slope efficiency

Figure 3 shows the output power dependencies on the pump power for the generations of LG_0^0 , LG_1^0 , and LG_2^0 laser modes. When the VWP is absent, the laser outputs a LCP LG_0^0 mode with a lasing threshold of approximately 0.5 W and a slope efficiency of 18.2%. Despite the extra loss induced by inserting the VWP, the threshold of the lasing LG_1^0 mode is only approximately 0.7 W with a corresponding slope efficiency of 11.06%. When the pump power increases to 1.7 W, the output power of the LG_1^0 mode reaches 120 mW. The lasing threshold is increased to 1.8 W for the LG_2^0 mode generation with a slope efficiency of 5.11%, because the loss due to the undesired modes generated by the VWP increases with the l value. Under the present experimental setup, the output power is limited by the damage thresholds of the components in the cavity. The intensity profiles are well preserved under different pump powers (see Appendix C). For generating high-power and/or higher-order LG modes, it is crucial to further improve the performances of the intracavity components, especially the conversion efficiency of the VWP.

B. Mode purities

Next, we present the transverse-mode-selection ability of the laser cavity by measuring the mode purities of the output LG_l^0 modes. We use a modal decomposition method to measure the purities of the output LG_l^0 laser modes under the output power of approximately 40 mW. One can see Refs. [24] and [40] for the detailed method. A group of pure LG_l^p modes with $p = 0-5$ and $l = 0, 1, 2$ are chosen to decompose the output LG_1^0 laser mode to determine its mode purity. Figure 4(a) shows the decomposing results in a histogram. The x axis and y axis represent the p index and l index, respectively, while the z axis shows the power weightings of different LG_l^p modes. The measured purity of the output LG_1^0 mode is 96.8%. Other undesired modes have been suppressed to near zero. To measure the output LG_2^0 laser mode, we choose a group of pure

LG_l^p modes with $p = 0-5$ and $l = 1, 2, 3$. The result shows the main power weighting of the LG_2^0 mode to be 92.7% [Fig. 4(b)]. The active cavity plays an important role in the transverse-mode selection, which increases the mode purities appreciably as compared to the achieved mode purities through extracavity modulation using VWPs (typically approximately 80% for the LG_1^0 mode and approximately 60% for the LG_2^0 mode) [24].

C. Laser output of cylindrical vector beams

Laser beams with different axial symmetries in polarization, the so-called cylindrical vector beams, can also be generated by different combinations of VWPs and linearly polarized directions of incident beams [38,41]. As shown in Fig. 1(a), a single VWP can achieve a reversible propagation cycle inside a laser cavity, which can be used to directly produce laser outputs of cylindrical vector beams.

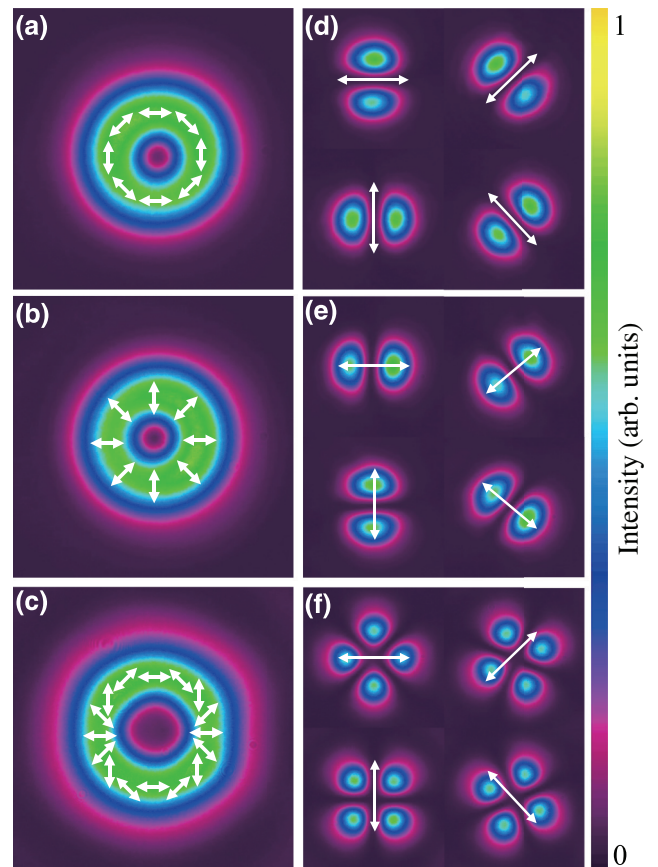


FIG. 5. Intensity patterns of cylindrical vector laser beams. Intensity patterns of the azimuthal (a) and radial (b) vector beams generated by a VWP of $m = 1$. (c) A higher-order cylindrical vector beam generated by a VWP of $m = 2$. (d)–(f) are the measured intensity distributions after passing through a linear polarizer oriented at different angles of 0° , 45° , 90° , and 135° , which correspond to (a)–(c), respectively. Arrows are used to indicate the polarization distributions in (a)–(c) and the orientations of the polarizer in (d)–(f).

Therefore, the new setup satisfies the self-reproducing and stability conditions for a cavity. The light beam incident on the VWP is fixed into a horizontal polarization in our experiment, so the output polarization distribution can be directly controlled by rotating the VWP to change φ_0 in Eq. (3). A linear polarizer is used to analyze the polarization distribution of the output beam. Figures 5(a) and 5(b) show the output cylindrical vector beams with a well-defined donut-intensity distribution by orienting the VWP of $m=1$ with different initial angles of $\varphi_0=45^\circ$ and $\varphi_0=0^\circ$, respectively. By orienting the linear polarizer at angles of 0° , 45° , 90° , and 135° , the measured intensity distributions are shown in Figs. 5(d) and 5(e), which indicate that the output beams shown in Figs. 5(a) and 5(b) are azimuthal and radial vector beams, respectively [42]. Using the VWP of $m=2$, we generate a higher-order cylindrical vector beam with negligible radial modes [Fig. 5(c)]. The measured intensity distributions after the linear polarizer, as shown in Fig. 5(f), reveal the cylindrical polarization distribution of Fig. 5(c). The cylindrical vector beams with a well-defined donut-intensity profile and controllable polarization distribution can be applied in optical communication, material processing, superfocusing, etc. [42–45].

IV. CONCLUSIONS

In summary, we have demonstrated a Nd:YVO₄ laser generating high-purity LG_l⁰ laser modes. The cavity design satisfies the light reversibility and stability conditions for a cavity, which plays a key role in efficient generation of a high-purity LG mode. The degeneracy of opposite-handedness LG modes is lifted through converting SAM into OAM for the field mode in the laser cavity. The output power dependencies on the pump power show low lasing thresholds (0.7 W for LG₁⁰ and 1.8 W for LG₂⁰) and high slope efficiencies (11.06% for LG₁⁰ and 5.11% for LG₂⁰) for the generated LG_l⁰ modes. The mode purities are up to approximately 97% and approximately 93% for the output LG₁⁰ and LG₂⁰ modes, respectively. The laser parameters are greatly improved in comparison to previous LG mode lasers. Changing the fast-axis orientation of the QWP, the generated LCP LG₋₁⁰ and LG₋₂⁰ modes have similar high-quality features as those of the LG₁⁰ and LG₂⁰ modes. The intensity profiles remain stable at different pump powers showing the mode stability of the cavity. Those features make the LG_l⁰ laser beam practical and the preferred choice for applications in optical tweezers, optical metrology, superresolution imaging, material processing, and so on. By further simplifying the cavity, different high-quality cylindrical vector beams have also been produced, which can be used in superfocusing and particle trapping. Less complexity in cavity construction and adjustment will allow our scheme to be easily transplanted into other laser and nonlinear systems, such as

Ti:Sapphire lasers, He-Ne lasers, CO₂ lasers, and even optical parametric oscillators. Furthermore, due to the flexible controllability of the azimuthal index and the low lasing threshold, it is possible to use such a setup to generate high-quality LG_l^p modes by replacing the VWP with LG_l^p modal q plates or J plates [46,47], which can be used to further increase the precision of gravitational-wave detection, extend high-dimensional entanglement and optical communication bandwidth, and design more sophisticated trapping configurations [19,20,25,48–50].

ACKNOWLEDGMENTS

This work was supported by National Key R&D Program of China (Grants No. 016YFA0302500 and No. 2017YFA0303703); National Natural Science Foundation of China (NSFC) (Grants No. 11874213, No. 91636106, and No. 11621091); Dengfeng Project B of Nanjing University.

APPENDIX A: SELF-REPRODUCING PROCESS

As shown in Figs. 1(c) and 1(d), a horizontally polarized OAM mode with a TC of l_0 passes through the FR with its polarization direction rotating 45° clockwise. The fast axis of the QWP is oriented horizontally so that the linearly polarized state turns into a LCP state. After passing through the VWP, the LCP state is reversed to a RCP state and an OAM mode with TC of l_0+m is generated as the output mode. Both the handedness of the circularly polarized state and the TC reverse again after the OAM mode is bounced back by the output coupler. Travelling back through the same VWP and QWP successively, the additional TC of the OAM mode is cancelled and the polarization direction has an angle of 135° with the initial polarization direction. In this process, the LCP OAM mode turns into a linearly polarized OAM mode with a TC of $-l_0$. Twisted by the FR again, the polarization state rotates 45° clockwise and recovers to the initial horizontal direction. The reflection of the front mirror inverses the TC to its initial value of l_0 , while keeping the horizontal polarization unchanged. Such a cycle repeats in the cavity. Similarly, orienting the fast axis of the QWP along the vertical axis, a LCP OAM mode with TC of $l_0 - m$ will be generated.

APPENDIX B: EXPERIMENTAL SETUP

As shown in Fig. 2(a), an a -cut 0.5 at. % Nd-doped YVO₄ crystal with dimensions of $3 \times 3 \times 8$ mm³ serves as the gain medium. One of its ends, acting as the front mirror, is coated with a reflectivity $>99.9\%$ at 1064 nm and a transmittance $>97.7\%$ at 808 nm; the other end has a high transmittance of $>99.8\%$ at 1064 nm. The crystal is mounted on a water-cooled copper holder maintained at room temperature and is oriented to generate horizontally polarized light. The output coupler is a plane mirror

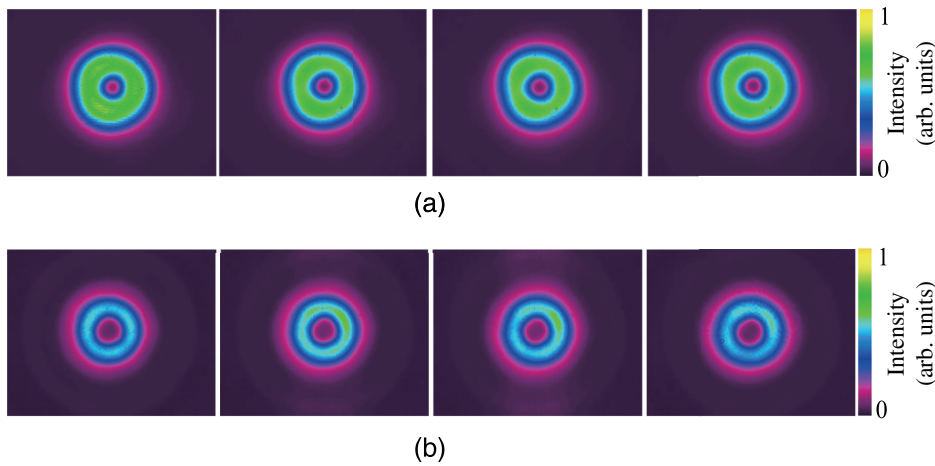


FIG. 6. Mode stability at different pump powers. (a) Intensity patterns of the LG_1^0 mode at the pump powers of 0.68, 1.10, 1.33 and 1.50 W, respectively. (b) Intensity patterns of the LG_2^0 mode at pump powers of 1.88, 2.49, 3.10, 3.60 W, respectively.

with a transmittance of 10% at 1064 nm. The lens with a focal length f is inserted into the cavity to ensure the cavity satisfies the stability condition. The pump source is a fiber-coupled laser diode outputting a continuous wave at an 808-nm wavelength, which is coupled out by a telescope and forms a 200 μm -diameter focusing spot in the crystal. The FR, QWP, and VWP are inserted into the laser cavity to achieve reversible mode conversion inside the cavity. The PBS next to the crystal eliminates unwanted vertically polarized light and the pinhole with a diameter of 1 mm suppresses the higher- p -order modes. To generate LG_1^0/LG_{-1}^0 (or LG_2^0/LG_{-2}^0) laser modes, we use a VWP of $m=1$ (or $m=2$). The cavity parameters are set to be $f=200$ mm, $L_A=205$ mm, and $L_B=45$ mm for LG_1^0/LG_{-1}^0 modes and $f=400$ mm, $L_A=380$ mm, and $L_B=45$ mm for LG_2^0/LG_{-2}^0 modes. The output laser beams are recorded by a laser beam profiler (LBP, Newport Corporation).

APPENDIX C: STABLE INTENSITY PROFILES

To demonstrate the excellent mode stability of the output LG_l^0 beams, we record the intensity patterns at a propagation distance of 50 cm at different pump powers. Figure 6(a) shows the intensity patterns of the LG_1^0 laser mode at pump powers of 0.68, 1.10, 1.33, and 1.50 W from left to right, respectively. The stable intensity patterns illustrate that increasing the pump power has little influence on the mode purity. The output LG_2^0 mode is robust as well, which can be seen from Fig. 6(b). The pump powers are 1.88, 2.49, 3.10, and 3.60 W from left to right, respectively.

[1] H. Kogelnik and T. Li, Laser beams and resonators, *Appl. Opt.* **5**, 1550 (1966).

- [2] A. Forbes, A. Dudley, and M. McLaren, Creation and detection of optical modes with spatial light modulators, *Adv. Opt. Photonics* **8**, 200 (2016).
- [3] L. Allen, M. W. Beijersbergen, R. J. Spreeuw, and J. P. Woerdman, Orbital angular momentum of light and the transformation of Laguerre-Gaussian laser modes, *Phys. Rev. A* **45**, 8185 (1992).
- [4] N. B. Simpson, K. Dholakia, L. Allen, and M. J. Padgett, Mechanical equivalence of spin and orbital angular momentum of light: An optical spanner, *Opt. Lett.* **22**, 52 (1997).
- [5] A. Mair, A. Vaziri, G. Weihs, and A. Zeilinger, Entanglement of the orbital angular momentum states of photons, *Nature* **412**, 313 (2001).
- [6] D. Wei, Y. Zhu, W. Zhong, G. Cui, H. Wang, Y. He, Y. Zhang, Y. Lu, and M. Xiao, Directly generating orbital angular momentum in second-harmonic waves with a spirally poled nonlinear photonic crystal, *Appl. Phys. Lett.* **110**, 261104 (2017).
- [7] X. Fang, G. Yang, D. Wei, D. Wei, R. Ni, W. Ji, Y. Zhang, X. Hu, W. Hu, Y. Q. Lu, S. N. Zhu, and M. Xiao, Coupled orbital angular momentum conversions in a quasi-periodically poled LiTaO₃ crystal, *Opt. Lett.* **41**, 1169 (2016).
- [8] A. Nicolas, L. Veissier, L. Giner, E. Giacobino, D. Maxein, and J. Laurat, A quantum memory for orbital angular momentum photonic qubits, *Nat. Photonics* **8**, 234 (2014).
- [9] N. Bozinovic, Y. Yue, Y. Ren, M. Tur, P. Kristensen, H. Huang, A. E. Willner, and S. Ramachandran, Terabit-scale orbital angular momentum mode division multiplexing in fibers, *Science* **340**, 1545 (2013).
- [10] J. Wang, J. Y. Yang, I. M. Fazal, N. Ahmed, Y. Yan, H. Huang, Y. X. Ren, Y. Yue, S. Dolinar, M. Tur, and A. E. Willner, Terabit free-space data transmission employing orbital angular momentum multiplexing, *Nat. Photonics* **6**, 488 (2012).
- [11] S. W. Hell and J. Wichmann, Breaking the diffraction resolution limit by stimulated emission: Stimulated-emission-depletion fluorescence microscopy, *Opt. Lett.* **19**, 780 (1994).
- [12] A. Alexandrescu, D. Cojoc, and E. Di Fabrizio, Mechanism of Angular Momentum Exchange Between Molecules

- and Laguerre-Gaussian Beams, *Phys. Rev. Lett.* **96**, 243001 (2006).
- [13] J. Hamazaki, R. Morita, K. Chujo, Y. Kobayashi, S. Tanda, and T. Omatsu, Optical-vortex laser ablation, *Opt. Express* **18**, 2144 (2010).
- [14] J. Arlt, M. MacDonald, L. Paterson, W. Sibbett, K. Dholakia, and K. Volke-Sepulveda, Moving interference patterns created using the angular Doppler-effect, *Opt. Express* **10**, 844 (2002).
- [15] J. Ni, C. Wang, C. Zhang, Y. Hu, L. Yang, Z. Lao, B. Xu, J. Li, D. Wu, and J. Chu, Three-dimensional chiral microstructures fabricated by structured optical vortices in isotropic material, *Light Sci. Appl.* **6**, e17011 (2017).
- [16] W. Yu, Z. Ji, D. Dong, X. Yang, Y. Xiao, Q. Gong, P. Xi, and K. Shi, Super-resolution deep imaging with hollow Bessel beam STED microscopy, *Laser Photonics Rev.* **10**, 147 (2016).
- [17] B. Mours, E. Tournefier, and J.-Y. Vinet, Thermal noise reduction in interferometric gravitational wave antennas: Using high order TEM modes, *Class. Quant. Grav.* **23**, 5777 (2006).
- [18] S. Chelkowski, S. Hild, and A. Freise, Prospects of higher-order Laguerre-Gauss modes in future gravitational wave detectors, *Phys. Rev. D* **79**, 122002 (2009).
- [19] V. D. Salakhutdinov, E. R. Eliel, and W. Löffler, Full-Field Quantum Correlations of Spatially Entangled Photons, *Phys. Rev. Lett.* **108**, 173604 (2012).
- [20] E. Karimi, D. Giovannini, E. Bolduc, N. Bent, F. M. Miatto, M. J. Padgett, and R. W. Boyd, Exploring the quantum nature of the radial degree of freedom of a photon via Hong-Ou-Mandel interference, *Phys. Rev. A* **89**, 013829 (2014).
- [21] M. Krenn, M. Malik, M. Erhard, and A. Zeilinger, Orbital angular momentum of photons and the entanglement of Laguerre-Gaussian modes, *Phil. Trans. R. Soc. A* **375**, 1 (2017).
- [22] A. M. Yao and M. J. Padgett, Orbital angular momentum: Origins, behavior and applications, *Adv. Opt. Photonics* **3**, 161 (2011).
- [23] E. Karimi, G. Zito, B. Piccirillo, L. Marrucci, and E. Santamato, Hypergeometric-gaussian modes, *Opt. Lett.* **32**, 3053 (2007).
- [24] B. Sephton, A. Dudley, and A. Forbes, Revealing the radial modes in vortex beams, *Appl. Opt.* **55**, 7830 (2016).
- [25] M. Granata, C. Buy, R. Ward, and M. Barsuglia, Higher-Order Laguerre-Gauss Mode Generation and Interferometry for Gravitational Wave Detectors, *Phys. Rev. Lett.* **105**, 231102 (2010).
- [26] R. N. Lanning, Z. Xiao, M. Zhang, I. Novikova, E. E. Mikhailov, and J. P. Dowling, Gaussian-beam-propagation theory for nonlinear optics involving an analytical treatment of orbital-angular-momentum transfer, *Phys. Rev. A* **96**, 013830 (2017).
- [27] Y. Senatsky, J. F. Bisson, J. L. Li, A. Shirakawa, M. Thiruganasambandam, and K. Ueda, Laguerre-Gaussian modes selection in diode-pumped solid-state lasers, *Opt. Rev.* **19**, 201 (2012).
- [28] A. Forbes, Controlling light's helicity at the source: Orbital angular momentum states from lasers, *Phil. Trans. R. Soc. A* **375**, 1 (2017).
- [29] D. Naidoo, K. Ait-Ameur, M. Brunel, and A. Forbes, Intracavity generation of superpositions of Laguerre-Gaussian beams, *Appl. Phys. B* **106**, 683 (2012).
- [30] A. A. Ishaaya, N. Davidson, and A. A. Friesem, Very high-order pure Laguerre-Gaussian mode selection in a passive Q-switched Nd : YAG laser, *Opt. Express* **13**, 4952 (2005).
- [31] I. A. Litvin, S. Ngcobo, D. Naidoo, K. Ait-Ameur, and A. Forbes, Doughnut laser beam as an incoherent superposition of two petal beams, *Opt. Lett.* **39**, 704 (2014).
- [32] D. Lin, J. M. Daniel, and W. A. Clarkson, Controlling the handedness of directly excited Laguerre-Gaussian modes in a solid-state laser, *Opt. Lett.* **39**, 3903 (2014).
- [33] D. J. Kim and J. W. Kim, Direct generation of an optical vortex beam in a single-frequency Nd : YVO₄ laser, *Opt. Lett.* **40**, 399 (2015).
- [34] D. Naidoo, F. S. Roux, A. Dudley, I. Litvin, B. Piccirillo, L. Marrucci, and A. Forbes, Controlled generation of higher-order Poincaré sphere beams from a laser, *Nat. Photonics* **10**, 327 (2016).
- [35] R. A. Beth, Mechanical detection and measurement of the angular momentum of light, *Phys. Rev.* **50**, 115 (1936).
- [36] K. Y. Bliokh, F. J. Rodríguez-Fortuño, F. Nori, and A. V. Zayats, Spin-orbit interactions of light, *Nat. Photonics* **9**, 796 (2015).
- [37] L. Marrucci, C. Manzo, and D. Paparo, Optical spin-to-orbital angular momentum conversion in inhomogeneous anisotropic media, *Phys. Rev. Lett.* **96**, 163905 (2006).
- [38] F. Cardano, E. Karimi, S. Slussarenko, L. Marrucci, C. de Lisio, and E. Santamato, Polarization pattern of vector vortex beams generated by q-plates with different topological charges, *Appl. Opt.* **51**, C1 (2012).
- [39] V. Magni, Resonators for solid-state lasers with large-volume fundamental mode and high alignment stability, *Appl. Opt.* **25**, 107 (1986).
- [40] T. Kaiser, D. Flamm, S. Schroter, and M. Duparre, Complete modal decomposition for optical fibers using CGH-based correlation filters, *Opt. Express* **17**, 9347 (2009).
- [41] M. Stalder and M. Schadt, Linearly polarized light with axial symmetry generated by liquid-crystal polarization converters, *Opt. Lett.* **21**, 1948 (1996).
- [42] Q. Zhan, Cylindrical vector beams: From mathematical concepts to applications, *Adv. Opt. Photonics* **1**, 1 (2009).
- [43] R. Dorn, S. Quabis, and G. Leuchs, Sharper Focus for a Radially Polarized Light Beam, *Phys. Rev. Lett.* **91**, 233901 (2003).
- [44] Z. Chen, Y. Zhang, and M. Xiao, Design of a superoscillatory lens for a polarized beam, *J. Opt. Soc. Am. B* **32**, 1731 (2015).
- [45] J. T. Barreiro, T. C. Wei, and P. G. Kwiat, Remote Preparation of Single-Photon "Hybrid" Entangled and Vector-Polarization States, *Phys. Rev. Lett.* **105**, 030407 (2010).
- [46] M. Rafayelyan and E. Brasselet, Laguerre-Gaussian modal q-plates, *Opt. Lett.* **42**, 1966 (2017).
- [47] R. C. Devlin, A. Ambrosio, N. A. Rubin, J. P. B. Mueller, and F. Capasso, Arbitrary spin-to-orbital angular momentum conversion of light, *Science* **358**, 896 (2017).
- [48] G. D. Xie, Y. X. Ren, Y. Yan, H. Huang, N. Ahmed, L. Li, Z. Zhao, C. J. Bao, M. Tur, S. Ashrafi, and A. E. Willner, Experimental demonstration of a 200-Gbit/s free-space

- optical link by multiplexing Laguerre-Gaussian beams with different radial indices, [Opt. Lett.](#) **41**, 3447 (2016).
- [49] M. Woerdemann, C. Alpmann, M. Esseling, and C. Denz, Advanced optical trapping by complex beam shaping, [Laser Photonics Rev.](#) **7**, 839 (2013).
- [50] P. Chen, L. L. Ma, W. Duan, J. Chen, S. J. Ge, Z. H. Zhu, M. J. Tang, R. Xu, W. Gao, T. Li, W. Hu, and Y. Q. Lu, Digitalizing self-assembled chiral superstructures for optical vortex processing, [Adv. Mater.](#) **30**, 1705865 (2018).